Nanoscale Advances

ROYAL SOCIETY OF CHEMISTRY

PAPER

View Article Online
View Journal | View Issue

Cite this: *Nanoscale Adv.*, 2020, **2**, 5648

Acetylated lignin nanoparticles as a possible vehicle for photosensitizing molecules†

Guillaume Marchand,[a] Gabin Fabre,[b] Nidia Maldonado-Carmona,[c] Nicolas Villandier[c] and Stéphanie Leroy-Lhez *[c]

Lignins are underused and abundant bio-sourced polymers with various potential applications. An attractive one is the development of nanoparticles for bioactive compound delivery. Here, we optimized the synthesis of hydrodispersible nanoparticles of acetylated lignin by comparing different lignin sources, degrees of acetylation and preparation methods. The formation of acetylated lignin nanoparticles in various solvents was probed by both experiments and, for the first time, a molecular dynamics simulation. We showed that dialysis is more suitable to obtain these nanoparticles than anti-solvent addition. The encapsulation of hydrophobic photosensitizing porphyrin in these nanoparticles was also demonstrated and rationalized at the molecular level, together with experiments, docking and molecular dynamics simulations. As acetylated lignin has been demonstrated to exhibit photosensitizing activity, the encapsulation of bioactive compounds in lignin nanoparticles opens the doors to a broad range of potential applications.

Received 28th July 2020
Accepted 12th October 2020

DOI: 10.1039/d0na00615g

rsc.li/nanoscale-advances

Introduction

Lignocellulosic biomass is an abundant renewable resource, mainly composed of cellulose, hemicelluloses and lignins. It appears to be a very interesting alternative to fossil resources for the production of biofuels and bio-based chemicals.[1–5]

Lignins are aromatic heteropolymers, derived mainly from radical polymerization of three monolignols: *p*-coumaryl, coniferyl and sinapyl alcohols.[6] They are the second most abundant renewable resource in nature, after cellulose, and comprise 25–30% of the non-fossil organic molecules on Earth.[7] They are mostly obtained or produced as a byproduct of pulping and in the paper-making industry. Of the 55–70 million tons produced annually, only 1–2% is used for the production of value-added products,[8] despite the fact that lignins exhibit low cytotoxicity, are biodegradable and have antioxidant, antimicrobial, anti-inflammatory and UV-blocking properties.[9–12] Lignins have the potential to be used in the treatment of obesity, diabetes, thrombosis, viral infections and cancer.[13] These biological activities convinced research teams to prepare micro- and nano-particles for bioactive compound delivery from unmodified or functionalized lignins. The materials obtained have found various applications in environmental science and medicine.[14–16] For example, in combination with other drugs, the biopolymer seems to be a good candidate for the development of solutions to fight against antimicrobial resistance.[17]

One alternative to increase the added value of products obtained from lignins is to modify them chemically. These modifications are generally carried out on the aromatic rings or aliphatic and phenolic hydroxyl groups present in the chemical structure of lignins.[18–20] Moreover, they can influence the physicochemical properties of lignins. As was reported in our previous work, acetylated lignins exhibit promising photosensitizing behavior in view of their ability to generate reactive oxygen species.[21] However, the various observations were made under organic solvent conditions. For this purpose, nanoparticles were prepared from two sources of softwood kraft acetylated lignins, named **AcKL-1** and **AcKL-2**, respectively, and through two different methods: by addition of an anti-solvent and by dialysis. Molecular dynamics simulations of lignin nanoparticles highlighted their solvent-dependent conformation, in correlation with experimental results. The influence of different experimental parameters on the final structure of these nano-objects as well as their stability was also studied. In order to enlarge the scope of their applications, the ability of these biologically sourced nanoparticles to encapsulate a bioactive molecule was also studied, both experimentally, and by docking and molecular dynamics simulations.

Experimental section

Reagents and solvents

Deionized water (resistivity ≥ 18 MΩ cm) used for the experiments conducted in this work was obtained from a Millipore

[a]*PEIRENE EA7500, Université de Limoges, Faculté de Pharmacie, 2 rue du Docteur Marcland, 87025 Limoges Cedex, France*

[b]*UMR 1248 INSERM, Université de Limoges, Faculté de Pharmacie, 2 rue du Docteur Marcland, 87025 Limoges Cedex, France*

[c]*PEIRENE EA7500, Université de Limoges, Faculté des Sciences, 123 rue du Albert Thomas, 87025 Limoges Cedex, France. E-mail: stephanie.lhez@unilim.fr*

† Electronic supplementary information (ESI) available: ESI1 includes supplementary experimental information, and ESI2 is a video of the molecular dynamics observations of nanoparticle formation. See DOI: 10.1039/d0na00615g

water purification system. Other reagents, except lignins and solvents, were purchased from various suppliers: Alfa Aesar, Sigma-Aldrich, and Fisher and were used without further purification.

Origin of kraft lignins KL-1 and KL-2

Both kraft lignins, **KL-1** and **KL-2**, are derived from softwoods. They were industrially precipitated from alkaline black liquors by acidification. **KL-1** was obtained from the supplier Sigma-Aldrich (supplier reference: 80068-05-1) and **KL-2** was generously donated by the Université du Québec à Trois-Rivières. The lignins were employed without prior purification.

Total acetylation of kraft lignins KL-1 and KL-2

Biopolymers were acetylated according to the method described by Marchand *et al.*[21] The two materials obtained from acetylation of **KL-1** and **KL-2** were named **AcKL-1** and **AcKL-2**, respectively.

Preparation of acetylated lignin nanoparticles

Two sets of nanoparticles were prepared from totally acetylated lignins, **AcKL-1** and **AcKL-2**, respectively. Each set of nanoparticles was prepared according to two different methods: either by dialysis (**NP-1** and **NP-2**) or by addition of an anti-solvent (**NP-1′** and **NP-2′**). Nanoparticles were also prepared by dialysis from partially acetylated materials $\mathbf{Ac_7KL\text{-}2}$, $\mathbf{Ac_{35}KL\text{-}2}$ and $\mathbf{Ac_{59}KL\text{-}2}$. The influence of different experimental parameters on the final structure of these nano-objects, as well as their stability, was studied.

Anti-solvent addition. The preparation was based on the work of Qian *et al.*[24] Acetylated lignins **AcKL-1** and **AcKL-2** were firstly dissolved in tetrahydrofuran (THF) at a concentration of 1 g L^{-1}. The solution was then stirred for 20 minutes and left to stand for three days in order to allow a good dispersion of the polymer, and thus a good subsequent structuring of the nanoparticles. Afterwards, two volumes of ultrapure water were added under magnetic stirring to the acetylated lignin solution at a flow rate of 18 mL h^{-1}. After water addition, the solution was filtered using a Millipore nylon filter (porosity 0.45 μm), and seven volumes of ultrapure water were added. The solution was finally left stirring in the open air overnight to allow the THF to evaporate.

Dialysis. The preparation by dialysis was based on various nanoparticle preparations already reported in the literature.[25–27] A fixed amount of acetylated or partially acetylated lignin (1 to 4 g L^{-1}) was first dissolved in a water-miscible organic solvent. The polymer solution was then introduced into a dialysis membrane with a porosity of 12 000 to 14 000 Da and dialyzed against 10 L of distilled water for 24 hours under low mechanical stirring. The nanoparticle solution was then centrifuged at 2740 × *g* for 20 min, and the supernatant was removed. This operation was repeated twice, and the nanoparticles were then dispersed into a fixed volume of water.

^{31}P NMR spectroscopy

^{31}P NMR analyses were performed at room temperature on a Bruker DPX 500 NMR spectrometer. The method described by Granata and Argyropoulos[23] was used. Cyclohexanol was used as an internal standard and chromium(III) acetylacetonate as a relaxation agent. NMR tubes were provided with coaxial inserts filled with 85% H_3PO_4 and all chemical shifts were reported relative to the signal of phosphoric acid.

FTIR spectroscopy

FT-IR spectra were obtained using a Frontier PerkinElmer spectrometer in the attenuation total reactance analysis mode. Spectra were collected between 600 and 4000 cm^{-1} after placing the pure product on a diamond crystal plate.

UV-Visible absorption spectroscopy

Acquisitions of UV-Visible absorption spectra were carried out between 300 and 800 nm on a Specord 210 Lambda double-beam spectrophotometer from Analytik Jena, using a 10 mm quartz cell.

Partial acetylation of kraft lignin KL-2

KL-2 was partially acetylated under stirring for 48 h at 25 °C in a mixture consisting of 10 mL of anhydrous pyridine and an equal volume of acetic anhydride, as described in the work of Buono *et al.*[22] At the end of the reaction, modified lignins were precipitated by the addition of ten volumes of distilled water, washed under vacuum with cold water and finally dried at 105 °C for 48 hours. FTIR and ^{31}P NMR analyses of the products showed clear signs of partial acetylation (see ESI1, Fig. S1 and S2†). More specifically, the study of the ^{31}P NMR spectra of partially acetylated lignins, after their functionalization, according to the method described by Granata and Argyropoulos,[23] allowed us to determine that 7, 35 and 59% of the hydroxyl groups of the respectively named $\mathbf{Ac_7KL\text{-}2}$, $\mathbf{Ac_{35}KL\text{-}2}$ and $\mathbf{Ac_{59}KL\text{-}2}$ lignins had been acetylated (see Tables 1, S1 and S2†).

Dynamic light scattering

Acquisitions of nanoparticle size distributions were performed on a Malvern Zetasizer Nano-ZS instrument. Measurements were carried out using a He–Ne laser at 663 nm, a wavelength where lignin absorbance is considered negligible,[40,41] thus avoiding any interactions that may lead to measurement errors. Three measurements, for lignins, were made on each sample at 20 °C using a light scattering angle of 173° and a refractive index of 1.59. The obtained DLS raw data were fit to a Gaussian model, excluding the values with less than 1% presence. The obtained data were validated through the analysis of their *R* square coefficient and through the analysis of the residuals with a D'Agostino & Pearson Omnibus K2 test. With this statistical approach, we obtained the mean size (geometrical mean) and the standard deviation (σ), which allowed us to approximate the range where 95% of the nanoparticles could be found (2σ).

Transmission electron microscopy

Analyses were carried out on two microscopes: a JEOL 100CX2 of 100 kV and a JEM-2100F of 200 kV. Immediately after ultrasonic

Table 1 Synthesis of partially acetylated lignins

Acetylated lignins	Starting material KL-2 (g)	Acetic anhydride (mL)	Acetic anhydride (eq.)	Pyridine (mL)	Mass yield (%)	Resulting acetylation rate (%)
Ac_7KL-2	2	0.180	0.22	10	95	7
Ac_{35}KL-2	2	0.472	0.57	10	96	35
Ac_{59}KL-2	2	0.700	0.85	10	103	59

dispersion, a drop of solution containing the material to be observed was deposited, on a 400 mesh copper grid with a 12 nm thick carbon membrane before analysis. No prior metallation of the samples was performed.

Scanning electron microscopy

Analyses were carried out on a ZEISS LEO1530VP. A drop of solution containing the material to be observed was deposited and dried on a sample holder. Prior platinum metallation of the samples was performed using an Agar Sputter Coater.

Acetylated lignin model preparation

For the investigation by computational chemistry, nine lignin models were used based on the work of Petridis *et al.*[28,29] The nine different lignin models all showed 61 guaiacyl units, but the models ranged from 0 to 6 branch points, representing the interunit-linkage of softwood lignin. All free hydroxyl groups were acetylated. Bonded and van der Waals parameters for the acetyl moiety were taken from the acetylated N-terminus (residue ACED in CHARMM36 (ref. 30)). Partial charges for the methyl part of the acetyl were also taken from residue ACED, while charges for the ester moiety were taken from an acetylated glycerol headgroup (residue GLYC, CHARMM36). In order to construct the coordinates for the different polymers, single units were added one by one using psfgen 1.6.4, a VMD[31] plugin. In order to prevent steric clashes by unit addition, in between each addition a short (10 ps) molecular dynamics (MD) simulation was run in a vacuum, in which the last unit added (in position N) was pulled away for the unit in position N – 4 along the polymer chain, with a force of 500 kJ mol^{-1} nm^{-1}. Thus, most of the polymer structure could relax while units were added at the tip of a branch of four residues, with enough empty space to avoid steric clashes during addition. All lignin models were further relaxed by simulated annealing MD simulations, in which the lignin was solvated in water molecules (TIP3P model[32]). The temperature of the lignin was linearly increased from 0 to 480 K in 1 ns, while the water was heated from 0 to 300 K. This cycle was repeated 100 times.

Encapsulation of THPP

The encapsulation of 5,10,15,20-tetrakis(4-hydroxyphenyl) porphyrin (**THPP**) was performed by dialysis. **AcKL-2** lignin was dissolved in acetone at a concentration of 2 g L^{-1} in the presence of the porphyrin at a concentration of 0.2 g L^{-1}. Acetone was chosen for these nanoparticle preparations because **THPP** is not soluble in THF. The solution obtained was then dialyzed against distilled water for 24 hours. The amount of porphyrin encapsulated in the nanoparticles was evaluated as follows: nanoparticles were centrifuged (2750 × *g*, 20 minutes) and washed with distilled water, and then, the nanoparticles were suspended in a fixed volume of water. A known volume of nanoparticles was dissolved in a known volume of acetone, to release the encapsulated molecules by destroying the structure of the nano-objects. The quantity of **THPP** was calculated in the acetone solution, and then extrapolated to the originally encapsulated THPP in the lignin nanoparticles, through UV-Visible absorption spectroscopy, by monitoring the absorbance at 419 nm. The concentration of **THPP** encapsulated in **NP-THPP** was then evaluated using the molar extinction coefficient of **THPP** (388 500 L mol^{-1} cm), calculated from standard solutions of **THPP** in acetone, with **THPP** concentrations ranging from 7.7×10^{-7} to 2.7×10^{-6} mol L^{-1}.

Docking calculations

In order to investigate possible preferential binding sites of **THPP** on the surface of lignin, docking calculations were performed using Autodock Vina.[33] For each lignin model, 1000 snapshots were taken at regular intervals during the 100 ns heating simulations. **THPP** was then docked on the whole polymer for each of these snapshots, with an exhaustiveness factor of 20. The energy range from the most to the least favorable poses was set to 5 kcal mol^{-1}.

Free molecular dynamics simulations

Free MD simulations were performed using Gromacs 5.1.[34] They were integrated using a 2 fs time step and the leap-frog Verlet scheme. Cutoffs for coulombic and van der Waals interactions were set to 1.2 nm, and particle mesh Ewald was used for long-range interactions. A switch function was used for van der Waals interactions between 0.9 and 1.0 nm. Temperature and pressure were kept constant at 298 K and 1 atm (isotropically). Periodic boundary conditions were used in every dimension. Bond constraints were handled by LINCS.[35] After an energy minimization using the steepest-descent algorithm, a 200 ps equilibration simulation was run with the v-rescale thermostat ($\tau_T = 0.1$ ps) and Berendsen barostat ($\tau_p = 1.0$ ps, compressibility $= 4.5 \times 10^{-5}$ bar^{-1}). Then, production MD simulations were run with identical parameters, except for the barostat which was Parrinello–Rahman with $\tau_p = 5.0$ ps.

The CHARMM force field for lignin and the TIP3P model were used for lignin and water. THF and acetone parameters were taken from the CHARMM36 force field.[30] **THPP** topology was obtained with the CgenFF program.[36,37]

Dialysis MD simulations

Dialysis was simulated by gradually replacing the initial solvent (acetone) with water during MD simulations. For this purpose, 100 cubic systems of solvent mixtures were prepared, in which the molar ratio of organic solvent (i) varied gradually from 0 to 100%. The volume V of each system was 27 nm^3. The initial number of water molecules ($N_{H_2O_i}$) in each mixture was determined according to eqn (1), based on experimentally determined densities for water–acetone mixtures (ρ_i).

$$N_{H_2O_i} = \frac{N_A \times V \times \rho_i}{M_{H_2O} + \frac{i}{1-i} \times M_{acetone}} \quad (1)$$

where N_A is the Avogadro constant, and M_{H_2O} and $M_{acetone}$ the molar weights of water and acetone, respectively. The densities (ρ_i) of the acetone–water mixtures were respectively fitted from ref. 38 to eqn (2) with $R^2 = 0.999$ and 0.996.

$$\rho_i = 173.21i^2 - 385.62i + 1000 \quad (2)$$

For each mixture, a 10 ns NPT simulation was performed and convergence of the density was ensured.

For the dialysis MD simulation, one unfolded lignin model was initially solvated with 100% acetone, along with 2 **THPP** molecules randomly placed in the solvent. The size of the dodecahedron box was adjusted so that the shortest distance between the lignin or **THPP** molecules to the edge of the box was 1.0 nm. During dialysis, every 5 ns, the solvent was removed, and the volume of the box was readjusted as mentioned above; this ensured that lignin did not interact with itself in the event of an unfolding, and allowed us to save computational time when lignin folded on itself. Then, the system was re-solvated in the next solvent mixture, *i.e.*, with 1% (mol/mol) less acetone. The thermostat and barostat during dialysis were identical to those in equilibration MD simulations.

Results and discussion

Solvent dependent conformation of lignin

To assess the behavior of acetylated lignin in water or in THF, free MD simulations were performed in those two solvents. First, the initial structures for the 9 acetylated lignin models were taken at the end of the simulated annealing simulations in water. After 100 ns of free MD simulation in water, the lignin models remained folded in small nanoparticles with an average diameter of 4.6 nm. This folding mimics the formation of NPs observed experimentally. Then, the water was stripped from the last structure of the free MD simulation, the lignin was resolvated in THF, and simulated for 100 ns (200 ns for L0a-acetyl).

For all these simulations, the solvent accessible surface area (SASA) was calculated and convergence was reached after 30 to 50 ns. SASA was averaged from 50 ns to the end of the simulations in water and in THF (Fig. S3†). It increased significantly in THF (152 ± 20 nm^2) compared to simulations in water (107 ± 5 nm^2). This indicates that acetylated lignin tends to form "crumpled globules" in water, and not in THF where it is soluble and unfolds. This is in good correlation with the previously reported behavior of native (non-acetylated) lignin.[39]

Additionally, no correlation was found between the number of branches in the lignin polymer (from 0 to 6 in 61 guaiacyl units) and SASA in either solvent (Fig. S4†). On the contrary, there was no significant difference between either SASA in water. This suggests that lignin adopts conformations of maximum packing in this solvent, where the SASA is minimized and thus it is independent of branching.

Determination of critical water concentration

Preparation of nanoparticles from acetylated lignin is based on the hydrophobicity of the modified lignins. During a gradual addition of water to a solution of lignins in a water-miscible organic solvent, the proportion of the organic solvent decreases. As a consequence, the lignin molecules begin to associate in the form of spheres to minimize hydrophobic interactions, until the formation of nanometric size particles, when the solvent is mainly composed of water. This progressive association can be demonstrated by measuring the intensity of the light scattered by an organic solution of lignins as a function of the volume of water added. The results obtained for **AcKL-1** and **AcKL-2** initially dissolved in THF are presented in Fig. 1. As the graph shows, for the two acetylated lignin solutions, the intensity of the scattered light increases suddenly from a water proportion of 30%, which is a sign that the polymer chains begin to aggregate. It should also be noted that the intensity of the scattered light increases more rapidly in the case of **AcKL-2** than **AcKL-1**, signifying that the association of lignins takes place more slowly in the latter case. This proportion of water, from which nanoparticles begin to form, is defined as the critical water concentration (CWC).[40] This concentration, although the same for the two lignins studied, is 10% lower than the one obtained by Qian *et al.*[24] These results are not surprising because Qian *et al.* used a lignin with a molar weight of 4200 g

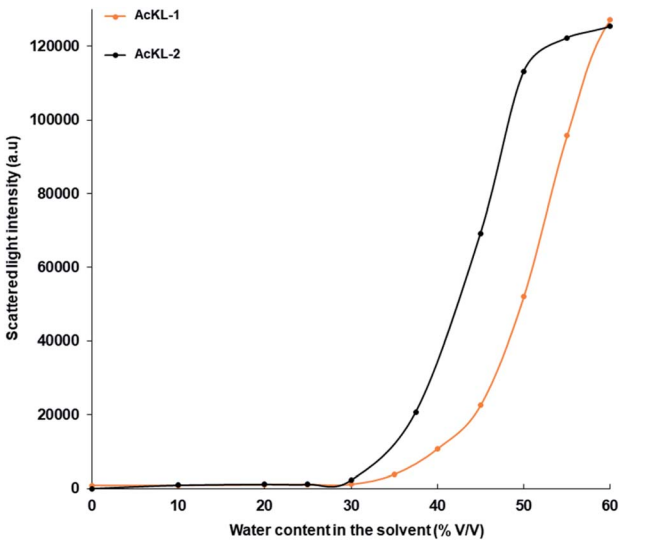

Fig. 1 Evolution of the scattered light intensity by acetylated lignin solutions in THF as a function of the quantity of added water.

mol^{-1} against lignins that are 13 100 and 9900 g mol^{-1} for **AcKL-1** and **AcKL-2**, respectively, and it has been previously described that the CWC of a polymer solution is a function of it molar mass.

The CWC was also evaluated with dialysis MD simulation, starting from 100% acetone. A decrease of the SASA was observed after the solvent mixture was 93% water (% mol_{water}/$mol_{acetone}$), which is equivalent to 76% water (% v_{water}/$v_{acetone}$) (Fig. S4†). The higher CWC compared to experimental results shown in Fig. 1 could be explained by the difference of solvent (THF *vs.* acetone) or by the difference of polymer molar mass.

Preparation of acetylated lignin nanoparticles

Nanoparticles were prepared from two sources of softwood kraft acetylated lignins, **AcKL-1** and **AcKL-2**, according to two different methods: by addition of an anti-solvent and by dialysis.

Anti-solvent addition. This method of preparation is based on the work of Qian *et al.*[24] and consists in a gradual addition of water to a THF solution of acetylated lignins. Nanoparticles were made according to this method, from acetylated lignins **AcKL-1** and **AcKL-2**, and respectively named **NP-1′** and **NP-2′**. For each source of lignin, preparations were made in ten replicates. The size distribution of the obtained nano-objects was then estimated for each case by DLS spectroscopy. Also, transmission electron microscopy analyses complemented these observations. Analysis of the size distribution of **NP-1′** and **NP-2′** (Fig. 2 and Table S3†) showed that both nanoparticles were obtained with mean sizes of 60.54 nm and 80.02 nm, while the distribution of 95% of the nanoparticle population (D_{95}) is found between 24.9 and 96.18 nm, and 30.18 and 129.86 nm, respectively. Thus, we can observe a slight variation in the mean size, depending on the starting material used. These observations were confirmed by transmission electron microscopy analysis. These results should be qualified in view of the low repeatability observed during the various preparations. Indeed, regardless of the starting material used, large standard deviations from the average particle diameters were observed.

Dialysis. This method of preparation consists in dissolving acetylated lignin in a water-miscible solvent such as THF or acetone, and in dialyzing the lignin solution against water. During this process, the organic solvent is gradually exchanged with water, resulting in the aggregation of acetylated polymer chains and thus leading to the formation of nanoparticles, as was described by molecular dynamics simulations. Nanoparticles were made according to this method from acetylated lignins **AcKL-1** and **AcKL-2** and respectively named **NP-1** and **NP-2**. Five preparations were made for each source of lignin. The size distributions of the nanoparticles obtained were estimated for each case by DLS spectroscopy (Fig. 2). The obtained mean sizes correspond to 157 nm and 163.3 nm, respectively, while their D_{95} is found to be between 45.82 and 268.18, and 52.18 and 274.42 nm, respectively. These observations were confirmed by transmission electron microscopy analysis (Fig. 2).

The two previously described methods have been compared, in order to choose the more suitable one for the preparation of nanoparticles, and especially to study their ability for drug encapsulation.

Although nanoparticles obtained by anti-solvent addition could be of smaller size than those obtained by dialysis, this first method has many disadvantages compared to dialysis, the first of them being that there is a high variance found between the samples (Fig. 2 and Table S1†). Indeed, the sizes observed

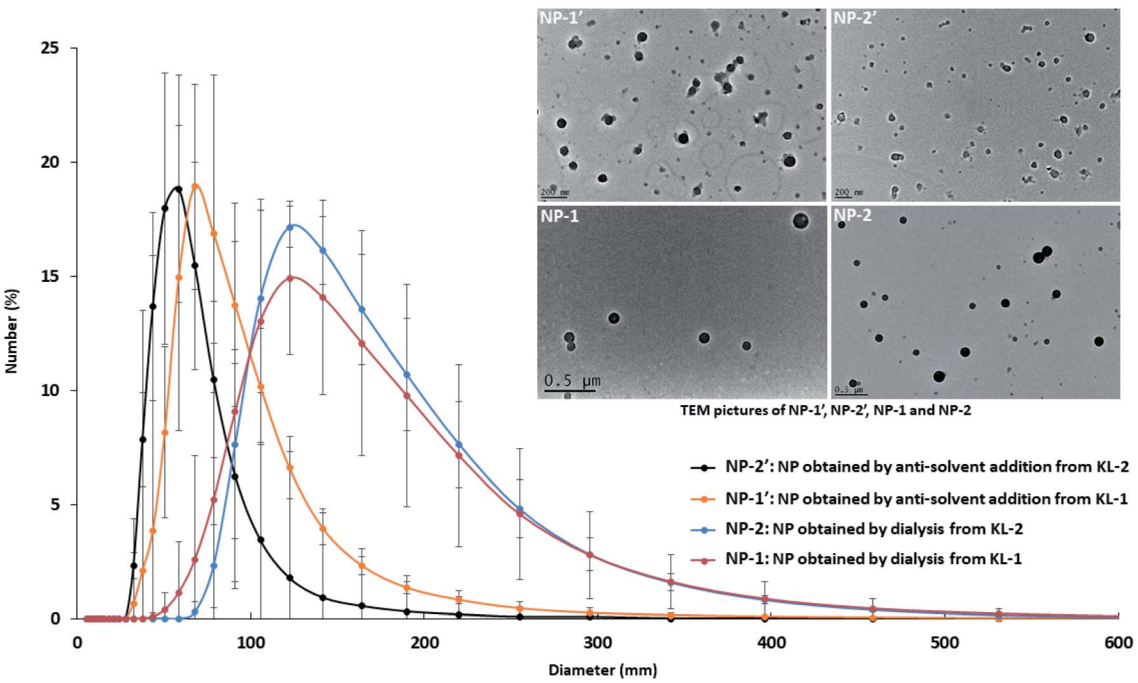

Fig. 2 Size distribution of NP-1′, NP-2′, NP-1 and NP-2. Inset: TEM pictures of NP-1′, NP-2′, NP-1 and NP-2.

for nanoparticles produced by the anti-solvent method vary significantly between the different syntheses, while the size of the nanoparticles obtained by dialysis is more constant. Therefore, this latter method allows us to work on populations of nanoparticles having relatively constant sizes.

SEM pictures (Fig. 3) confirm these observations and clearly show that several populations of nanoparticles, with different morphologies, were obtained by the anti-solvent method, while the ones obtained by dialysis are relatively similar in their shape, size and morphology.

In addition, the anti-solvent method involved a filtration step, in which a large proportion of the nanoparticles were retained on the filter. This provoked a mass concentration of lignin nanoparticles, not only too low, but also too complex to determine. This method therefore does not seem appropriate for the production of nanoparticles for biological activity measurements, where nano-objects have to be in sufficient and known quantity. Conversely, dialysis not only allowed the preparation of nanoparticles in sufficient quantity, but also the estimation of the mass concentration in solution. Indeed, no significant loss of material was observed by this method of preparation. To ensure this, **NP-2** solutions were lyophilized, and the mass of each residue was determined. These masses were found to be substantially identical to the masses of lignins initially introduced into the dialysis membranes since the observed mass loss is less than 1% (Table S4†).

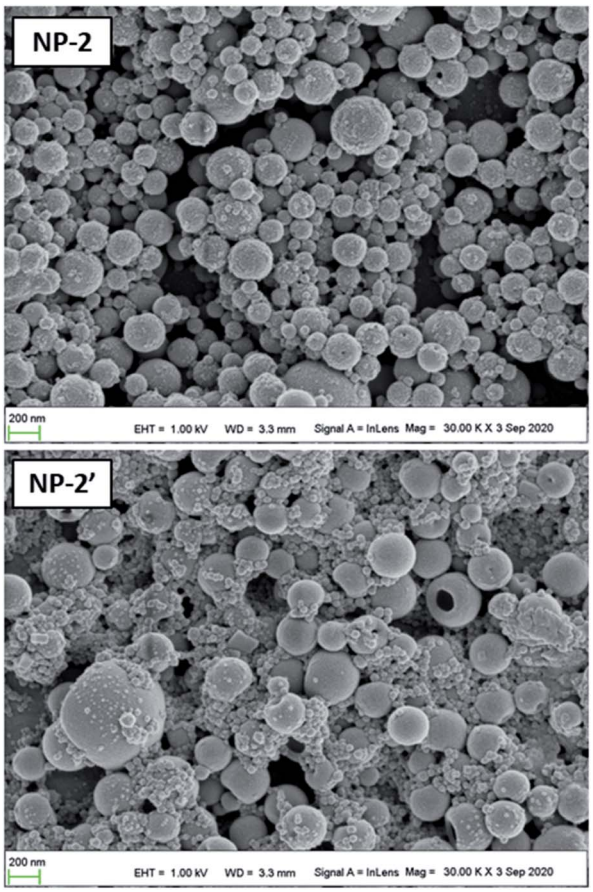

Fig. 3 SEM pictures of NP-2 and NP-2′.

Finally, the production of nanoparticles by dialysis has the advantage of being, experimentally, the simpler of the two methods. Indeed, it requires fewer steps than the anti-solvent method. Moreover, it is not necessary to leave the acetylated lignin solution for three days before the nanoparticle preparation step as various tests have shown that only twenty minutes of stirring is necessary for a good future structuring of the nanoparticles.

In conclusion, dialysis, by making it possible to obtain nanoparticles in a simple and repeatable manner, appeared to be the most suitable method for the preparation of nanoparticles of acetylated lignins.

Stability of lignin nanoparticles prepared by dialysis

In order to test the stability and endurance of the acetylated lignin nanoparticles, we subjected them to several treatments. One of the key steps in the preparation of lignin nanoparticles is their centrifugation to collect and concentrate them. During this step, nanoparticles are subjected to high centrifugal forces. It is therefore fundamental to know if the nanoparticles can endure this stage. Transmission electron microscopy observations showed that no degradation of acetylated lignin nanoparticles was observed after centrifugation up to 10 000 × *g*. Furthermore, TEM pictures (Fig. S5†) showed that nanoparticles keep their spherical shape after this step. The stability of nanoparticles was also evaluated over time. The size distribution of **NP-2** was measured regularly by DLS spectroscopy for 36 days. The analysis of the results did not reveal any degradation of the nanoparticles over this period. Considering the advantages outlined in previous paragraphs and the stability that **NP-2** demonstrated during and after centrifugation and over time, dialysis was retained as the method of choice for the preparation of acetylated lignin nanoparticles in the rest of this work.

Separation of nanoparticle populations by centrifugation

We have demonstrated so far the feasibility of our method for the preparation of acetylated lignin nanoparticles. However, the obtained nanoparticles have a heterogeneous distribution of sizes, which could diminish their potential for further applications. Thus, it was demonstrated that nanoparticles could be separated through differential centrifugal speeds, thus allowing nanoparticle populations with a narrower size distribution to be obtained. Therefore, after being prepared by dialysis, nanoparticles were centrifuged under the normal centrifugation conditions (2740 × *g*, 20 minutes). The supernatant was recovered and centrifuged at a higher speed (5480 × *g*, 20 minutes); the obtained nanoparticles were recovered, and the supernatant was treated in the same way at 8220 and 8768 × *g*, for 20 minutes each. The recovered nanoparticle pellets were then suspended in distilled water and analyzed by DLS. The size distributions of the obtained nanoparticles were compared in Fig. 4.

It was observed that with an increasing applied centrifugal force, the mean size decreased from 253.2 nm to 66.18 nm. Also, a decrease of the D_{95} was observed when we compared the D_{95}

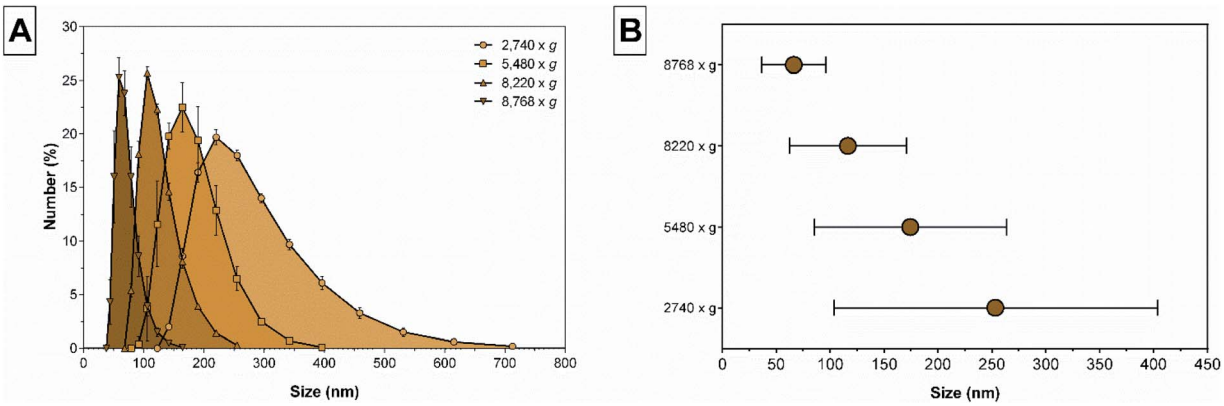

Fig. 4 (A) Distribution curves for the obtained nanoparticles at different centrifugal forces; (B) mean size obtained for nanoparticles at different centrifugal forces.

with an applied centrifugal speed of 2740 × *g* (103.36 nm to 403.4 nm) to that when 8768 × *g* was applied (36.46 to 95.9 nm). These analyses demonstrated that using differential centrifugation speeds allows nanoparticles with decreasing mean size and increasingly tight population distributions to be collected. So, although normally a relatively wide distribution of size of nanoparticles is obtained, smaller fractions can also be obtained by a simple modification of the centrifugation procedure.

Optimization of the preparation by dialysis

To complete the study on this method of preparation, we evaluated various factors that can influence the structure of nanoparticles of acetylated lignins. Herein, we will only focus on **NP-2** nanoparticles.

The influence of the solvent in which the acetylated lignins are initially dissolved was evaluated. The **AcKL-2** material was dissolved at a concentration of 2 g L^{-1} in various organic solvents: acetone, dimethylformamide (DMF) and dimethylsulfoxide (DMSO), all three being water-miscible. Each preparation was made in triplicate. No nanoparticle was formed when **AcKL-2** was initially dissolved in DMF or DMSO, while nanoparticles (**NP-2-Atn**) were obtained with acetone. However, nanoparticles could also be obtained from a mixture of THF and DMSO, at a 8 : 2 proportion. The nanoparticles obtained indicated that the addition of DMSO to the mixture increased the nanoparticles' mean size from 124.7 to 184.6 nm, but a more drastic effect is observed on the width of the D_{95} distribution, going from a basal 54 to 195.4 nm to 12.06 to 357.14 nm when DMSO is added to the mixture. Nevertheless, nanoparticles formed from a starting solution of THF or acetone, and both solutions had similar size distribution profiles (Fig. S6†). These various findings were confirmed by scattering and transmission electron microscopy (Fig. S7 and S8†). SEM analysis also showed that the morphology of nanoparticles prepared with acetone is not different from that prepared using THF, thus making it possible to validate the use of acetone and THF as solvents for the preparation of acetylated lignin nanoparticles. Also, the use of DMSO as a mixture is possible, but the mean size and D_{95} range are increased (Table 2). However, the choice of a more polar solvent, like DMSO, may enable the encapsulation of highly insoluble compounds, such as phthalocyanines and porphyrins.

The influence of the mass concentration of acetylated lignins in the starting solution was also studied. **AcKL-2** was dissolved to obtain concentrations of 1, 2 and 4 g L^{-1} in THF. The size

Table 2 Characteristics of nanoparticles based on acetylated lignins, as a function of the solvent, the starting concentration and the degree of acetylation of lignins

Acetylated lignins	Starting concentration (g L^{-1})	Acetylation rate (%)	Solvent	NP formation	Mean size (nm)	Distribution range with 95% of the nanoparticles (D_{95})
AcKL-2	2	100	THF	Yes	163.3	45.82–268.18
			Acetone	Yes	146.7	56.8–236.6
			DMSO	No	—	—
			DMF	No	—	—
			DMSO : THF 8 : 2	Yes	184.6	12.06–357.14
	1	100	THF	Yes	156.2	42.64–269.76
	4	100	THF	Yes	227.2	79.12–375.28
Ac_7KL-2	2	7	THF	Yes	95.04	45.8–144.28
Ac_{35}KL-2	2	35	THF	Yes	107.1	43.92–170.28
Ac_{59}KL-2	2	59	THF	Yes	102.8	43.76–161.84

distributions of the nanoparticles formed, respectively named **NP-2** (1 g L^{-1}),**NP-2** (2 g L^{-1}) and **NP-2** (4 g L^{-1}), were analyzed by DLS spectroscopy (Fig. S9†) and results are reported in Table 2. Each preparation was made in triplicate.

NP-2 (4 g L^{-1}) exhibited a medium size of around 227.2 nm, which is significantly higher than that of **NP-2** (1 g L^{-1}) and **NP-2** (2 g L^{-1}), which were respectively equal to 156.2 and 163.3 nm. In addition, the particle size distribution of **NP-2** (4 g L^{-1}) extended over a much larger range than **NP-2** (1 g L^{-1}) and **NP-2** (2 g L^{-1}) as the D_{95} of **NP-2** (4 g L^{-1}) is wider (79.12 to 375.28 nm) than the **NP-2** (1 g L^{-1}) and **NP-2** (2 g L^{-1}) distributions (42.64 to 269.76 nm and 52.18 to 274.42 nm, respectively). The results indicated that the nanoparticles obtained, whether with 2 g L^{-1} or 1 g L^{-1}, share the same distribution and mean size. Nevertheless, nanoparticles prepared with a starting solution of 2 g L^{-1} were routinely prepared, as more nanoparticles could be obtained from the same batch and with the same quality.

The effect of the degree of lignin acetylation on nanoparticle formation was also investigated. For this purpose, three partially acetylated lignins, respectively at 7% (**Ac_7KL-2**), 35% (**Ac_{35}KL-2**) and 59% (**Ac_{59}KL-2**), were dissolved in THF to achieve a concentration of 2 g L^{-1}. The size distributions of the nanoparticles formed, respectively named **NP(Ac_7KL-2)**, **NP(Ac_{35}KL-2)** and **NP(Ac_{59}KL-2)**, were measured and compared with that of the fully acetylated **NP-2** nanoparticles (Fig. S10†). As shown in Table 2, the nanoparticles formed from partially acetylated materials have similar mean diameters: 95.04, 107.1 and 102.8 nm for **NP(Ac_7KL-2)**, **NP(Ac_{35}KL-2)** and **NP(Ac_{59}KL-2)**, respectively. These mean diameters appeared to be smaller than the ones obtained for nanoparticles made from totally acetylated lignins. Moreover, the size distributions of nanoparticles prepared from partially acetylated lignins were narrower than that of **NP-2**. Indeed, D_{95} of nanoparticles prepared from partially acetylated lignins ranges between 40 and 170 nm. The incomplete acetylation of the polymers therefore seems to favor the formation of nanoparticles of smaller sizes. These results agreed with those presented by Qian *et al.*[24] whereby the authors obtained particles with similar sizes by preparing them *via* the addition of an anti-solvent to solutions of partially acetylated lignins (82 and 94%) in THF. SEM pictures of **Ac_7KL-2** (Fig. S11†) show that, apart from the size, the nanoparticles prepared from partially acetylated lignins do not show any differences in morphology compared to those prepared from fully acetylated lignins.

THPP encapsulation

In order to validate the feasibility of the encapsulation of hydrophobic bioactive compounds in acetylated lignin nanoparticles, a poorly water-soluble model compound, 5,10,15,20-tetrakis(4-hydroxyphenyl)porphyrin, abbreviated **THPP** (Fig. 5), was encapsulated. This compound also has the advantage of having a distinguishable UV-Visible spectrum, facilitating the monitoring of its encapsulation. The encapsulation of **THPP** was performed *via* dialysis according to the work described by Figueiredo *et al.*,[41] on the encapsulation of sorafenib and capecitabine in lignin and metal-complexed lignin nanoparticles. The obtained nanoparticles (abbreviated **NP-THPP**) were characterized by DLS spectroscopy (Fig. 6A), scattering electron microscopy (Fig. 6B) and transmission electron microscopy (Fig. S12†).

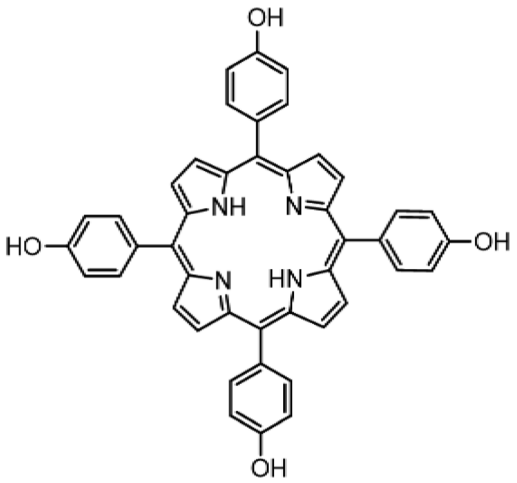

Fig. 5 Chemical structure of 5,10,15,20-tetrakis(4-hydroxyphenyl) porphyrin (THPP).

NP-THPP nanoparticles were smaller (99.17 nm) than **NP-2-Atn** nanoparticles (146.7 nm). Additionally, a narrower distribution is found for **NP-THPP** (43.47 to 154.87 nm) than the distribution observed for **NP-2-Atn** (56.8–236.6 nm). This feature should indicate a strong interaction between nanoparticles and **THPP**. SEM analysis (Fig. 6B) shows that the morphology of **NP-THPP** is not different from that of **NP-2-Atn**. An encapsulation yield of 0.13 (±0.02) mmol of **THPP** per gram of lignin was determined by UV-Vis measurement at 419 nm, a wavelength where lignin light absorption is negligible. This encapsulation level corresponds to an encapsulation of 85 ± 12% of the **THPP** initially introduced. This value is quite similar to those obtained by Figuerido *et al.*,[41] respectively of 75% ± 10% and 68% ± 19% for capecitabine and sorafenib.

The stability of the encapsulation of **NP-THPP** was tested over time. A freshly prepared batch of **NP-THPP** was suspended in phosphate buffer (pH 7.0) and stored away from light. Periodically, a fraction of these nanoparticles was centrifuged (10 000 × *g*, 30 minutes), and both the supernatant and the centrifuged nanoparticles were analyzed through their UV-Vis spectra. Leaking of **THPP** on phosphate buffer is found only after ten days of suspension, but the leaked amount remained the same after 60 days. This leakage can be attributed to **THPP** found on the outermost part of the nanoparticles, where **THPP** is retained by weak interactions with lignins, and so is more susceptible to leaking out (Fig. 6C). Other methods, reported in the literature, where porphyrinic compounds were intended to be transported through lignin[42] or through other biopolymeric matrices,[43] generally involved chemical modification of the porphyrin in order to avoid undesired leaking. Thus, the present formulation seems to be able to encapsulate porphyrinic compounds, without further chemical modifications.

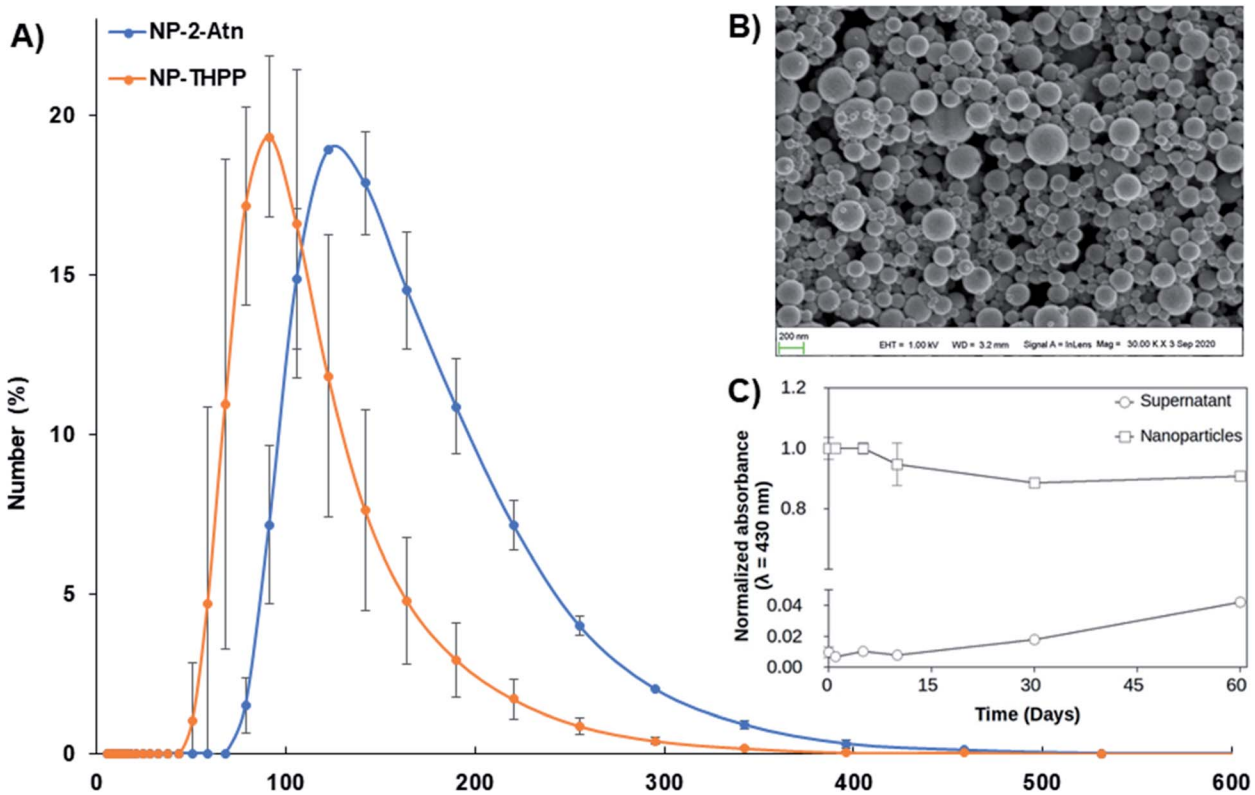

Fig. 6 (A) Size distributions of NP-2Atn and NP-THPP; (B) SEM picture of NP-THPP; (C) release of THPP from NP-2 over time.

Interaction of THPP at the surface of lignin nanoparticles

To evaluate the possible use of acetylated lignin nanoparticles as carriers for hydrophobic compounds, the interaction between **THPP** and lignin nanoparticles was investigated *in silico* by docking and molecular dynamics simulations.

For each lignin model, 1000 structures were taken from the simulated annealing simulations, and **THPP** was docked on these 1000 structures for each lignin model. Docking calculations showed no significant difference of affinity distribution between lignin models (Fig. S13†). No significant difference in average binding affinity was measured when performing time block analysis (10 blocks corresponding to 10 ns of simulated annealing simulation, Table S5†). Small differences were observed for the best docking affinity for each model (from -9.9 kcal mol^{-1} for L6-acetyl to -11.5 kcal mol^{-1} for L0a-acetyl); however these differences are smaller than the reported accuracy of Autodock Vina (2.85 kcal mol^{-1}). Moreover, the proportion of poses with a docking affinity lower than 9.0 kcal mol^{-1} was 0.8%, and these poses correspond to very short-lived lignin structures in the simulated annealing simulations (less than 1 ns). The spatial and temporal repartition of docking poses were visualized by projecting the density of **THPP** atoms on the lignin nanoparticle surface (ESI2, Video S1†). From one lignin conformation to the other, the position of the best docking poses fluctuated widely. Therefore, there is no specific binding site of **THPP** at the surface of lignin nanoparticles, and the interaction is independent of the lignin model used. This non-specificity correlates with the fractal and fluid nature of the lignin surface previously reported.[44]

Docking affinities suggest a strong interaction between **THPP** and lignin nanoparticles. These results were confirmed by MD simulations in water, where **THPP** molecules were initially placed in water, far from the nanoparticles. For every lignin model, all **THPP** molecules moved to the lignin nanoparticle surface in less than 10 ns. The position adopted by **THPP** molecules at the surface of lignin nanoparticles was the closest from the starting position in water. Then they stayed in the same position at the surface for the rest of the 100 ns simulations. This confirms the strong affinity of **THPP** for the lignin nanoparticle surface, and the lack of specific binding sites.

In order to assess whether **THPP** could be encapsulated inside the lignin polymer during dialysis rather than being located at its surface, 2 **THPP** molecules were added at the beginning of the dialysis simulation. These apolar molecules only started to interact with the acetylated lignin surface at around the CWC, *i.e.*, 76% (v/v) water in the solvent. At the end of the dialysis both molecules were located at the surface of the NP, and not encapsulated inside the polymer globules (Fig. 7). Both **THPP** molecules were close to each other on the surface, favoring π–π stacking between them. This suggests that stable **THPP** molecules, that did not leak during experimental measurements, were trapped in between different polymers forming a NP, rather than inside individual polymers.

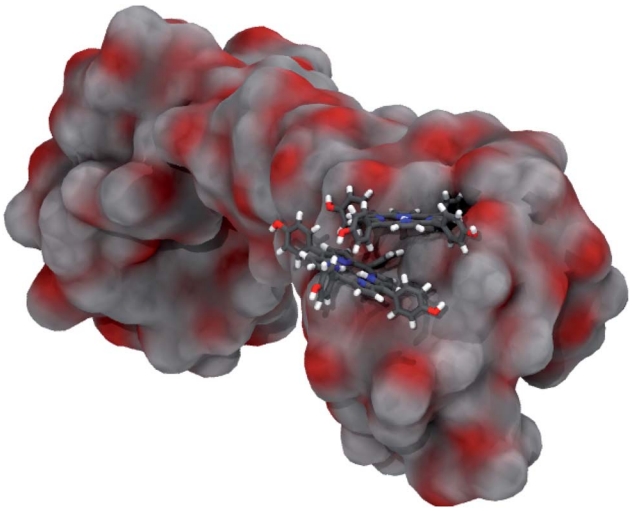

Fig. 7 Position of the THPP molecules at the surface of the L0a-acetyl NP at the end of the dialysis simulation.

Molecular description of the encapsulation in lignin nanoparticles

As the suspensions of **NP-1** and **NP-2** in water were stable over time, we can assume that their density is close to that of water. However, taking into account their respective average diameters (157 nm and 163.3 nm) and the molar weight of the acetylated lignin polymers (13 100 and 9900 g mol^{-1} for **AcKL-1** and **AcKL-2**, respectively), we find that the nanoparticles must consist of 9 $\times$ 10^4 to 1.4 $\times$ 10^5 individual polymers, aggregated during dialysis.

Assuming that these individual lignin polymers are spheres, the sum of their surfaces in one nanoparticle is about 4 μm^2, while the exterior surface of the spherical nanoparticle is about 0.08 μm^2. The ratio of the exterior surface to the total surface is therefore 2%. As the docking and MD simulations showed, **THPP** molecules are located at the surface of these polymers, with no specific binding site. Thus, the uniform repartition of **THPP** molecules at the surface of the polymers while nanoparticles aggregate during dialysis indicates that about 2% of **THPP** is located at the surface of lignin nanoparticles. The remainder is encapsulated inside the nanoparticle, between polymers. This correlates with the 2% increase of absorbance in the supernatant after 30 days (Fig. 6C). Therefore, this suggests that the leakage of **THPP** over time arises from the **THPP** molecules located at the surface of the nanoparticle, while **THPP** that is hidden at the surface of the polymers inside the nanoparticle remains encapsulated.

Conclusions

Acetylated lignin nanoparticles appear to be an economical and easy-to-prepare formulation. The procedure for preparing and obtaining the nanoparticles by dialysis indeed demonstrated its robustness, as we were able to obtain nanoparticles under several solvent conditions and substitutional degrees of lignin. Acetylated lignin nanoparticles seem to be an appropriate vehicle for the delivery of small photosensitizer molecules. Experiments so far had demonstrated the ease of their preparation, being reproducible and quite stable as suspensions. The present experiments and our previous evidence of the photosensitizing activity of acetylated lignins may provide a powerful tool for photodynamic applications. The biological role of nanoparticles loaded with photosensitizing molecules is an interesting topic that is currently being addressed in our research group, as an antibacterial treatment. Future work includes the encapsulation of other porphyrinic compounds, the analysis of their spectrophotometric and photophysical properties, and also a more detailed analysis of their endurance under several conditions. Furthermore, we expect that this formulation will have broader applications, as an oxidant of small molecules in aqueous media, an application with an environmental impact.

Conflicts of interest

There are no conflicts to declare.

Acknowledgements

We thank the "Conseil Régional du Limousin" and European Union for their financial support. Indeed, this work is a part of the ITN-EJD-2017 project POLYTHEA which has received funding from the European Union's Horizon 2020 research and innovation programme under the Marie Sklodowska-Curie grant agreement no. 764837. The authors are indebted to Dr Pierre Carles for TEM analysis, Eloise Hyvernaud for SEM analysis and Dr Yves Champavier for the NMR analysis. The authors thank CALI and its team that supported the molecular modelling calculations; CALI is the calculation center of the University of Limoges, funded by Région Limousin, the European Union, University of Limoges, and XLIM, IPAM, and GEIST research institutes. GF thanks Loukas Petridis for providing the lignin force field. The authors also thank Daire Gibbons for his help in improving the English of this paper.

References

1 F. H. Isikgor and C. Remzi Becer, *Polym. Chem.*, 2015, **6**, 4497–4559.
2 R. A. Sheldon, *Green Chem.*, 2014, **16**, 950–963.
3 A. Corma, S. Iborra and A. Velty, *Chem. Rev.*, 2007, **107**, 2411–2502.
4 G. W. Huber, S. Iborra and A. Corma, *Chem. Rev.*, 2006, **106**, 4044–4098.
5 J. N. Chheda, G. W. Huber and J. A. Dumesic, *Angew. Chem., Int. Ed.*, 2007, **46**, 7164–7183.
6 W. Boerjan, J. Ralph and M. Baucher, *Annu. Rev. Plant Biol.*, 2003, **54**, 519–546.
7 V. K. Thakur, M. K. Thakur, P. Raghavan and M. R. Kessler, *ACS Sustainable Chem. Eng.*, 2014, **2**, 1072–1092.
8 R. Rinaldi, R. Jastrzebski, M. T. Clough, J. Ralph, M. Kennema, P. C. A. Bruijnincx and B. M. Weckhuysen, *Angew. Chem., Int. Ed.*, 2016, **55**, 8164–8215.

9 V. Ugartondo, M. Mitjans and M. P. Vinardell, *Bioresour. Technol.*, 2008, **99**, 6683–6687.
10 A. Barapatre, A. S. Meena, S. Mekala, A. Das and H. Jha, *Int. J. Biol. Macromol.*, 2016, **86**, 443–453.
11 O. Gordobil, R. Herrera, M. Yahyaoui, S. İlk, M. Kaya and J. Labidi, *RSC Adv.*, 2018, **8**, 24525–24533.
12 G. J. Gil-Chávez, S. S. P. Padhi, C. V. Pereira, J. N. Guerreiro, A. A. Matias and I. Smirnova, *Int. J. Biol. Macromol.*, 2019, **136**, 697–703.
13 M. P. Vinardell and M. Mitjans, *Int. J. Mol. Sci.*, 2017, **18**, 1219.
14 M. H. Sipponen, H. Lange, C. Crestini, A. Henn and M. Österberg, *ChemSusChem*, 2019, **12**, 2038.
15 S. Iravani and R. S. Varma, *Green Chem.*, 2020, **22**, 612–636.
16 P. Figueiredo, K. Lintinen, J. T. Hirvonen, M. A. Kostiainen and H. A. Santos, *Prog. Mater. Sci.*, 2018, **93**, 233–269.
17 N. Maldonado-Carmona, T.-S. Ouk, M. J. F. Calvete, M. M. Pereira, N. Villandier and S. Leroy-Lhez, *Photochem. Photobiol. Sci.*, 2020, **19**, 445–461.
18 D. Kai, M. J. Tan, P. L. Chee, Y. K. Chua, Y. L. Yap and X. J. Loh, *Green Chem.*, 2016, **18**, 1175–1200.
19 C. Wang, S. S. Kelley and R. A. Venditti, *ChemSusChem*, 2016, **9**, 770–783.
20 S. Sen, S. Patil and D. S. Argyropoulos, *Green Chem.*, 2015, **17**, 4862–4887.
21 G. Marchand, C. A. Calliste, R. M. Williams, C. McLure, S. Leroy-Lhez and N. Villandier, *ChemistrySelect*, 2018, **3**, 5512–5516.
22 P. Buono, A. Duval, P. Verge, L. Averous and Y. Habibi, *ACS Sustainable Chem. Eng.*, 2016, **4**, 5212–5222.
23 A. Granata and D. S. Argyropoulos, *J. Agric. Food Chem.*, 1995, **43**, 1538–1544.
24 Y. Qian, Y. Deng, X. Qiu, H. Li and D. Yang, *Green Chem.*, 2014, **16**, 2156.
25 S. Salentinig and M. Schubert, *Biomacromolecules*, 2017, **18**, 2649–2653.
26 Y. Qian, Y. Deng, H. Li and X. Qiu, *Ind. Eng. Chem. Res.*, 2014, **53**, 10024–10028.
27 M. Lievonen, J. J. Valle-Delgado, M.-L. Mattinen, E.-L. Hult, K. Lintinen, M. A. Kostiainen, A. Paananen, G. R. Szilvay, H. Setälä and M. Österberg, *Green Chem.*, 2016, **18**, 1416–1422.
28 L. Petridis, R. Schulz and J. C. Smith, *J. Am. Chem. Soc.*, 2011, **133**, 20277–20287.
29 L. Petridis and J. C. Smith, *J. Comput. Chem.*, 2009, **30**, 457–467.
30 J. Huang and A. D. MacKerell, *J. Comput. Chem.*, 2013, **34**, 2135–2145.
31 W. Humphrey, A. Dalke and K. Schulten, *J. Mol. Graphics*, 1996, **14**, 33–38.
32 W. L. Jorgensen, J. Chandrasekhar, J. D. Madura, R. W. Impey and M. L. Klein, *J. Chem. Phys.*, 1983, **79**, 926–935.
33 O. Trott and A. J. Olson, *J. Comput. Chem.*, 2010, **31**, 455–461.
34 M. J. Abraham, T. Murtola, R. Schulz, S. Páll, J. C. Smith, B. Hess and E. Lindahl, *SoftwareX*, 2015, **1–2**, 19–25.
35 B. Hess, H. Bekker, H. J. C. Berendsen and J. G. E. M. Fraaije, *J. Comput. Chem.*, 1997, **18**, 1463–1472.
36 K. Vanommeslaeghe, E. Hatcher, C. Acharya, S. Kundu, S. Zhong, J. Shim, E. Darian, O. Guvench, P. Lopes, I. Vorobyov and A. D. MacKerell, *J. Comput. Chem.*, 2010, **31**, 671–690.
37 K. Vanommeslaeghe and A. D. MacKerell, *J. Chem. Inf. Model.*, 2012, **52**, 3144–3154.
38 K. T. Thomas and R. A. McAllister, *AIChE J.*, 1957, **3**, 161–164.
39 M. D. Smith, B. Mostofian, X. Cheng, L. Petridis, C. M. Cai, C. E. Wyman and J. C. Smith, *Green Chem.*, 2016, **18**, 1268–1277.
40 L. Zhang and A. Eisenberg, *Polym. Adv. Technol.*, 1998, **9**, 677–699.
41 P. Figueiredo, K. Lintinen, A. Kiriazis, V. Hynninen, Z. Liu, T. Bauleth-Ramos, A. Rahikkala, A. Correia, T. Kohout, B. Sarmento, J. Yli-Kauhaluoma, J. Hirvonen, O. Ikkala, M. A. Kostiainen and H. A. Santos, *Biomaterials*, 2017, **121**, 97–108.
42 H.-Y. Tse, S.-C. Cheng, C. S. Yeung, C.-Y. Lau, W.-H. Wong, C. Dong and S.-Y. Leu, *Green Chem.*, 2019, **21**, 1319–1329.
43 C. Ringot, N. Saad, F. Brégier, P. Bressollier, E. Poli, V. Chaleix, T. S. Ouk and V. Sol, *Photochem. Photobiol. Sci.*, 2018, **17**, 1780–1786.
44 L. Petridis, S. V. Pingali, V. Urban, W. T. Heller, H. M. O'Neill, M. Foston, A. Ragauskas and J. C. Smith, *Phys. Rev. E: Stat., Nonlinear, Soft Matter Phys.*, 2011, **83**, 061911.

